ARCHIVES OF METALLURGY AND MATERIALS
Volume 52 2007 Issue 2

K. KOWALCZYK-GAJEWSKA*, Z. MRÓZ*, R. B. PĘCHERSKI*, **

MICROMECHANICAL MODELLING OF POLYCRYSTALLINE MATERIALS UNDER NON-PROPORTIONAL DEFORMATION PATHS

MODELOWANIE MIKROMECHANICZNE MATERIAŁÓW POLIKRYSTALICZNYCH DLA NIEPROPORCJONALNYCH ŚCIEŻEK DEFORMACJI

The rigid-plastic crystal plasticity model with single yield surface of 2n-degree is applied to simulate the polycrystalline behaviour and the crystallographic texture development under non-proportional deformation paths. The role of two controlling parameters: the amplitude and frequency for the processes of tension or compression assisted by cyclic torsion of thin-walled tubes made of copper is analysed. The effect of micro-shear bands on the reduction of global hardening rate is described by means of the contribution function of shear banding in the rate of plastic deformation. The conclusions drawn from the study can find also application in the extension of the analysis for high strength and hard deformable materials.

Przeprowadzono symulacje zachowania się polikryształu oraz rozwoju tekstury krystalograficznej dla nieproporcjonalnych ścieżek deformacji wykorzystując sztywno-plastyczny model plastyczności kryształu z powierzchnią plastyczności stopnia $2n$. Przeanalizowano wpływ dwóch parametrów kontrolnych: amplitudy i częstości dla procesów rozciągania lub ściskania przy udziale cyklicznego skręcania cienkościennych rurek wykonanych z miedzi. Efekt działania mikropasm ścinania w postaci redukcji globalnego modułu wzmocnienia odkształceniowego został opisany poprzez funkcję udziału pasm ścinania w przyroście deformacji plastycznej. Wnioski wysnute z powyższego studium mogą znaleźć docelowo zastosowanie w rozszerzeniu analizy dla materiałów o podwyższonej wytrzymałości oraz materiałow trudno odkształcalnych.

1. Motivation

Metal forming processes such as extrusion assisted by cyclic torsion have demonstrated essential advantages with respect to classical forming processes. The significant reduction of required load for forming, growth of ductility, possible reduction of dissipated energy of forming and finer grain structure are the main beneficial factors, cf. e.g. [5, 10, 11]. One of possible explanations of these advantages is the appearance of a multi-scale hierarchy of shear localization modes, so-called shear banding, that replaces the crystallographic multiple slip or twinning and reduces strain hardening. In the paper the constitutive model developed in [13] will be applied to study macroscopic behaviour of polycrystalline materials that are subjected to non-proportional deformation paths as so called KOBO-type processes related with cyclic torsion [10]. Plastic anisotropy evolution connected with crystallographic texture development will be also studied.

In the next section the concise description of the constitutive model is given. More information can be found in [12] and [13]. In section 3 the results of numerical simulation are presented and discussed. Finally, in the last section the conclusions are outlined.

2. The constitutive modelling

2.1. The single grain model with the yield surface of 2n-degree

The rigid-plastic model is considered. In order to study the texture development as well as the polycrystalline behaviour for the advanced plastic deformation process the large strain formulation of the crystal plasticity theory has to be applied [3]. We use the multiplicative decomposition of the total deformation gradient into the elastic part and the plastic part $\mathbf{F}^p$. The assumption is made that the elastic stretches are negligible comparing

* INSTITUTE OF FUNDAMENTAL TECHNOLOGICAL RESEARCH PAS, 00-049 WARSZAWA, 21 ŚWIĘTOKRZYSKA STR., POLAND
** INSTITUTE OF STRUCTURAL MECHANICS, FACULTY OF CIVIL ENGINEERING, CRACOW UNIVERSITY OF TECHNOLOGY, 31-155 KRAKÓW, 24 WARSZAWSKA STR., POLAND

to the analysed plastic strains so that the elastic part is restricted to the rigid rotation $\mathbf{R}^*$. It is easy to show that such form of the deformation gradient results in the additive decomposition of the velocity gradient $\mathbf{L}$ into the elastic spin $\mathbf{\Omega}^*$, the plastic spin $\mathbf{\Omega}^p$ and the rate of plastic deformation tensor $\mathbf{D}^p$ (the symmetric part of the plastic part of the velocity gradient)

$$\mathbf{L} = \mathbf{\Omega}^* + \mathbf{\Omega}^p + \mathbf{D}^p. \tag{2.1}$$

It is generally accepted that during the elastic regime crystallographic lattice and the material undergo the same deformation while plastic deformation does not induce lattice motion which is described only by the elastic spin. Plastic deformation occurs by slip in the specified crystallographic direction $\mathbf{m}$ on the specified crystallographic plane with the unit normal $\mathbf{n}$. The number M and type of slip systems $\{\mathbf{n}, \mathbf{m}\}$ depend on the lattice type. In this paper the numerical simulations are performed for the f.c.c. crystals with 12 slip systems $\{111\} < 110 >$. The plastic part of the velocity gradient is then described as follows

$$\mathbf{L}^p = \mathbf{\Omega}^p + \mathbf{D}^p = \sum_{r=1}^{M} \dot{\gamma}^r \mathbf{m}^r \otimes \mathbf{n}^r \tag{2.2}$$

In the classical Schmid multi-surface plasticity the slip on the considered slip system is initiated if the resolved shear stress $\tau^r = \mathbf{m}^r \cdot \boldsymbol{\sigma} \cdot \mathbf{n}^r$ reaches the critical value τ_c^r being the material parameter. Instead of this formulation the regularized Schmid law (the crystal plasticity with single yield surface) is used [12]. In view of this model the crystallographic slip mechanism is activated when the following yield condition for the Cauchy stress $\boldsymbol{\sigma}$ is fulfilled

$$f(\boldsymbol{\sigma}) = \frac{1}{2n} \sum_{r=1}^{M} \left(\frac{\tau^r}{\tau_c^r} \right)^{2n} - m = 0, \tag{2.3}$$

where n is the positive exponent and m is the material parameter independent of the lattice orientation [7]. The rate of plastic deformation tensor is associated with this yield condition

$$\mathbf{D}^p = \dot{\lambda} \sum_{r=1}^{M} \frac{1}{\tau_c^r} \left(\frac{\tau^r}{\tau_c^r} \right)^{2n-1} \mathbf{P}^r \tag{2.4}$$

and for the plastic spin $\mathbf{\Omega}^p$ the following specification is used

$$\mathbf{\Omega}^p = \dot{\lambda} \sum_{r=1}^{M} \frac{1}{\tau_c^r} \left(\frac{\tau^r}{\tau_c^r} \right)^{2n-1} \mathbf{W}^r, \tag{2.5}$$

where $\mathbf{P}^r$ and $\mathbf{W}^r$ are symmetric and skewsymmetric parts of $\mathbf{m}^r \otimes \mathbf{n}^r$ diad, respectively. Comparing the above flow rules with the kinematic description (2.2) one may easily identify that

$$\dot{\gamma}^r = \dot{\lambda} \frac{1}{\tau_c^r} \left(\frac{\tau^r}{\tau_c^r} \right)^{2n-1}. \tag{2.6}$$

In its mathematical structure this model is similar to the rate-dependent formulation [4], however, the reference velocity, which is the material parameter in the latter approach, is here replaced by the plastic multiplier $\dot{\lambda}$ obtained from the consistency condition for the yield surface (2.3). The explicit formula for $\dot{\lambda}$ may be found in [7]. In the case of deformation controlled process it may be calculated from the formula

$$\dot{\lambda} = \frac{\|\mathbf{D}^p\|}{\| \sum_{r=1}^{M} \frac{1}{\tau_c^r} \left(\frac{\tau^r}{\tau_c^r} \right)^{2n-1} \mathbf{P}^r \|},$$

where $\|\mathbf{A}\| = \sqrt{\mathbf{A} \cdot \mathbf{A}} = \sqrt{A_{ij} A_{ij}}$.

Slip occurs by motion of dislocations that have to overcome both short-range and long-range obstacles. Accumulation of dislocations makes its further movement more and more difficult. This qualitative description of physical nature of slip is captured in the framework of crystal plasticity by the hardening rule for the critical resolved shear stress τ_c^r. In this study we use the formula proposed in [3]

$$\dot{\tau}_c^r = \sum_{q=1}^{M} h_{rq} |\dot{\gamma}^q|, \tag{2.7}$$

where hardening matrix h_{rq} enables to account for the latent and self-hardening by setting the parameter $q \neq 1$ in its specification

$$h_{rq} = h_q (q + (1 - q)\delta_{rq}).$$

For the function h_q responsible for the self-hardening we assume the following equation [2]

$$h_q = h_o \left| 1 - \frac{\tau_c^q}{\tau_{sat}} \right|^{\beta} \tag{2.8}$$

with the material parameters $\{h_o, \tau_{c0}^q, \tau_{sat}, \beta\}$ that have to be identified in the experiments. Here τ_{c0}^r are the initial values of τ_c^q.

Most of the results discussed in this paper is obtained applying the presented model. The material parameters have been identified with use of the experimental results for polycrystalline copper reported in [9], [1]. They have been obtained by fitting the stress-strain curve for the simple compression. More details concerning the identification procedure may be found in [14].

2.2. Simplified description of the reduction of the hardening rate due to micro shear bands

General conclusion that follows from experiments [5, 10, 11] is that by persistent changing of the deformation path it is possible to reduce significantly the global strain hardening rate. The inventors of KOBO method explained their pivotal idea as follows. Experience gained from the conducted tests allow them to argue that the change of mode of plastic flow destabilizes the material substructure that has been developed and leads to the initiation of the second mode of deformation. The homogeneous crystallographic slip is gradually replaced by the localized heterogeneous deformation by micro-shear bands.

In order to account for the reduction of the hardening rate due to appearance of micro-shear bands we follow the concept introduced in [18]. The plastic velocity gradient $\mathbf{L}^p$ is decomposed into two parts: one connected with the crystallographic slip $\mathbf{L}^p_{slip}$ and one connected with micro-shear bands $\mathbf{L}^p_{MS}$. For the crystallographic slip the rate-independent single grain model presented in the previous subsection is used. The constitutive approach for the part connected with the micro-shear bands was thoroughly described in the series of papers [13, 18–21].

In the present analysis the simplified model describing the effect of micro-shear bands is applied. The yield condition for initiation of micro-shear bands is the same as the yield condition for slip mechanism (2.3). In [13] two flow rules for micro-shear bands were considered. In this paper we focus on the model in which the flow rule for the part of the rate of plastic deformation $\mathbf{D}^p_{MS}$ connected with micro-shear bands is associated with the yield condition, so both tensors $\mathbf{D}^p_{MS}$ and $\mathbf{D}^p_{slip}$ have the same directions. Using the following notation:

$$\|\mathbf{D}^p\| = d, \quad \|\mathbf{D}^p_{slip}\| = d_{slip},$$
$$\|\mathbf{D}^p_{MS}\| = d_{MS} \Rightarrow f_{MS} = \frac{d_{MS}}{d}$$

the total rate of plastic deformation reads

$$\mathbf{D}^p = \frac{\dot{\lambda}}{1 - f_{MS}} \sum_{r=1}^{M} \frac{1}{\tau^r_c} \left(\frac{\tau^r}{\tau^r_c}\right)^{2n-1} \mathbf{P}^r, \quad f_{MS} \in < 0, 1) \quad (2.9)$$

and the constitutive function f_{MS} describes the contribution of shear banding in the rate of plastic deformation.

Since the hardening rate depends on the increment of crystallographic slip (Eqs (2.6) and (2.7)), the higher contribution of micro-shear bands the higher is the reduction of the global strain hardening rate. According to the invoked experimental results the reduction of strain hardening is more pronounced for plane strain compression than for the simple compression [9]. Following this observation the f_{MS} function of logistic dependence on accumulated plastic strain proposed and identified in [19], [16], was extended in [13] to incorporate the effect of the type of strain path so that the following formula was proposed

$$f_{MS}(\xi) = \frac{f^{\infty}_{MS}}{1 + \exp(a - b\xi)},$$

where

$$\xi = \sqrt{\frac{3}{2}} \varepsilon^p_{eq} (1 - \alpha |\cos 3\theta|), \quad 0 \leqslant \alpha \leqslant 1 \qquad (2.10)$$

and

$$\dot{\varepsilon}^p_{eq} = \sqrt{\frac{2}{3} \mathbf{D}^p \cdot \mathbf{D}^p}, \quad |\cos 3\theta| = 3\sqrt{6} |\det(\boldsymbol{\mu}_{\mathbf{D}^p})|,$$
$$\boldsymbol{\mu}_{\mathbf{D}^p} = \frac{\mathbf{D}^p}{\|\mathbf{D}^p\|}.$$

The coefficient α is an additional material parameter that describes the following ratio

$$\alpha = 1 - \frac{\xi_{\cos 3\theta = 1}}{\xi_{\cos 3\theta = 0}}$$

for the same value of the accumulated plastic strain for two extreme types of strain paths. In the next section the non-proportional strain paths will be analysed, therefore, contrary to the analysis in [13] the distinction has to be made between magnitude of plastic strain $\|\mathbf{E}^p\|$ and the accumulated plastic strain ε^p_{eq}. For the purpose of this analysis the second one must be used.

For the plastic spin connected with micro-shear bands we use the rule expressed in [6] that relates the plastic spin to the non-coaxiality factor between corresponding the plastic strain rate tensor and the C a u c h y stress

$$\boldsymbol{\Omega}^p_{MS} = \omega \bar{f}_{MS} \frac{\mathbf{D}^p_{MS}\boldsymbol{\sigma} - \boldsymbol{\sigma}\mathbf{D}^p_{MS}}{\|\mathbf{D}^p_{MS}\boldsymbol{\sigma} - \boldsymbol{\sigma}\mathbf{D}^p_{MS}\|}, \qquad (2.11)$$

where

$$\|\boldsymbol{\Omega}^p\| = \omega, \quad \|\boldsymbol{\Omega}^p_{MS}\| = \omega_{MS} \quad \Rightarrow \bar{f}_{MS} = \frac{\omega_{MS}}{\omega}.$$

For the second constitutive function $\bar{f}_{MS}$ connected with micro-shear bands two possibilities are considered, namely

$$\bar{f}_{MS} = 0, \quad \text{and} \quad \bar{f}_{MS} = f_{MS}. \qquad (2.12)$$

In the first case there is no plastic spin due to micro-shear banding and in the second case the contribution of

micro-shear bands mechanism to the total plastic spin is the same as the contribution to the rate of plastic deformation tensor.

The material parameters $\{a, b, f_{MS}^{\infty}, \alpha\}$ connected with the incorporation of shear banding have been identified by comparison of the experimental results for simple compression and plane strain compression reported in [9], [1].

3. Simulations

3.1. Program of simulations

In the simulations non-proportional deformation paths are studied. The analysis is performed at the material point on the level of a polycrystalline sample. As the representative volume element (RVE) for this macroscopic material point, the grain aggregate composed of 500 grains with initially random distribution of lattice orientations is assumed. As a micro-macro transition rule the Taylor hypothesis is applied assuming that the velocity gradient $\mathbf{L}^g$ in every grain is the same and equal to the macroscopic velocity gradient $\mathbf{L}$. The macroscopic stress and plastic dissipation are calculated as follows

$$\mathbf{\Sigma} = \sum_{g=1}^{N} \nu^g \boldsymbol{\sigma}^g, \quad \dot{W}^p = \sum_{g=1}^{N} \nu^g \boldsymbol{\sigma}^g \cdot \mathbf{D}^p \Rightarrow W^p = \int_0^t \dot{W}^p dt, \tag{3.13}$$

where ν^g is the volume fraction of grains with the orientation g in RVE.

Consider a thin walled tube of initial outer radius R_o, length L_o and wall thickness t_o subjected to axial tension or compression, Fig. 1. Assume the axial strain rate $\dot{\varepsilon}_x$ to be specified and constant. The alternating torsion is imposed in order to reduce the axial stress and the applied axial force in order to execute the process. Such processes of tension or compression assisted by cyclic torsion were studied in [15] in the framework of small strain formalism and rigid-plastic or elastic-plastic material model with the H u b e r-V o n M i s e s yield condition.

Here these processes will be studied in the framework of large strain formalism and crystal plasticity. In order to do that the macroscopic velocity gradient of the form

$$L_{ij} = \dot{\varepsilon}_x \begin{bmatrix} \pm 1.0 & 0 & 0 \\ \eta(t) & \mp 0.5 & 0 \\ 0 & 0 & \mp 0.5 \end{bmatrix} \quad \text{in} \quad \{\mathbf{e}_k\} \tag{3.14}$$

is assumed where $\dot{\varepsilon}_x$ is the constant rate of extension while $\eta(t)\dot{\varepsilon}_x$ is the rate of shear in cyclic torsion. Similarly to [15] piecewise linear and harmonic programs of cyclic torsion will be considered that is

$$\eta(t) = \begin{cases} \eta_0 \text{sign}[\cos(2\pi t/T)] \\ \frac{\pi}{2}\eta_o \cos(2\pi t/T) \end{cases} \tag{3.15}$$

and

$$E = \dot{\varepsilon}_x T,$$

where η_o controls the maximum rate of shear. The resulting stress-strain curves will allow us to compare the influence of the process parameters $\{\eta_o, \gamma_m\}$ on the axial stress reduction and the plastic dissipation. The texture evolution will allow to study the microstructure changes. The simulations have been performed for the set of controlling parameters collected in Table 1. The calculations have also been done for $\eta_o = 0$. The analysed set of parameters roughly corresponds to the program of experiments performed by G r o s m a n and P a w l i c k i [8] on cylinders made of copper. For the upper row of η_o values the maximum shear angle γ_m is close to 2^o and for the lower row it is close to 8^o.

TABLE 1
Set of controlling parameters for the simulation program

	Strain period $E = \varepsilon_x T$		
	0.085	0.031	0.013
η_o	1.64	4.56	10.54
	6.56	18.2	42.2

The deformation history may be derived using the known relation

$$\dot{\mathbf{F}} = \mathbf{L}\mathbf{F}, \quad \dot{F}_{ij}(t) = L_{ik}(t) F_{kj}(t)$$

which actually consists of 9 differential equations. They can be integrated to obtain

$$F_{ij} = \begin{bmatrix} \exp(\pm\varepsilon_x) & 0 & 0 \\ f(\varepsilon_x)\exp\left(\mp\frac{1}{2}\varepsilon_x\right) & \exp\left(\mp\frac{1}{2}\varepsilon_x\right) & 0 \\ 0 & 0 & \exp\left(\mp\frac{1}{2}\varepsilon_x\right) \end{bmatrix} \quad \text{in} \quad \{\mathbf{e}_k\}, \tag{3.16}$$

where $\varepsilon_x = \dot{\varepsilon}_x t$ and in the case of harmonic torsion oscillations

$$f(\varepsilon_x) = \frac{\pi\eta_o E}{16\pi^2 + 9E^2}$$
$$\left[\exp\left(\pm\frac{3}{2}\varepsilon_x\right)\left(3E\cos(2\pi\frac{\varepsilon_x}{E}) \pm 4\pi\sin(2\pi\frac{\varepsilon_x}{E})\right) - 3E\right].$$

The initial conditions of the form $\mathbf{F}(0) = \mathbf{I}, \quad F_{ij}(0) = \delta_{ij}$ have been assumed. In the case of piecewise linear oscillations it is obtained for the regimes of constant η

$$f(\varepsilon_x) = F_{12}^0\exp(\frac{1}{2}\varepsilon_0) \pm \frac{2\eta}{3}\left(\exp(\frac{3}{2}\varepsilon_x) - \exp(\frac{3}{2}\varepsilon_0)\right),$$

where $F_{12}(\varepsilon_0) = F_{12}^0$ and $\varepsilon_x = \varepsilon_0$ indicates the moment of last reversing of torsion deformation.

Using the specified deformation gradient (3.16) one may derive stretch ratios along axis of a tube and along the tube radius (see Fig. 1)

$$\lambda_1 = \exp(\pm\varepsilon_x)\sqrt{1 + f^2(\varepsilon_x)\exp(\mp 3\varepsilon_x)},\ \lambda_3 = \exp\left(\mp\frac{1}{2}\varepsilon_x\right)$$

as well as sinus of an angle of shear Γ between initially perpendicular directions $\mathbf{e}_1$ and $\mathbf{e}_2$ (see Fig. 2)

$$\sin\Gamma = \frac{f(\varepsilon_x)\exp(\mp\frac{3}{2}\varepsilon_x)}{\sqrt{1 + f^2(\varepsilon_x)\exp(\mp 3\varepsilon_x)}}.$$

Finally, the rate of equivalent plastic strain $\dot{\varepsilon}_{eq}^p$ in the analysed case (compare (2.1)) reads

$$\dot{\varepsilon}_{ep}^p = \dot{\varepsilon}_x\sqrt{1 + \frac{1}{3}\eta^2}$$

so the results presented in the next subsection must be interpreted with care because axial plastic strain is for the considered process not equal to the equivalent plastic strain.

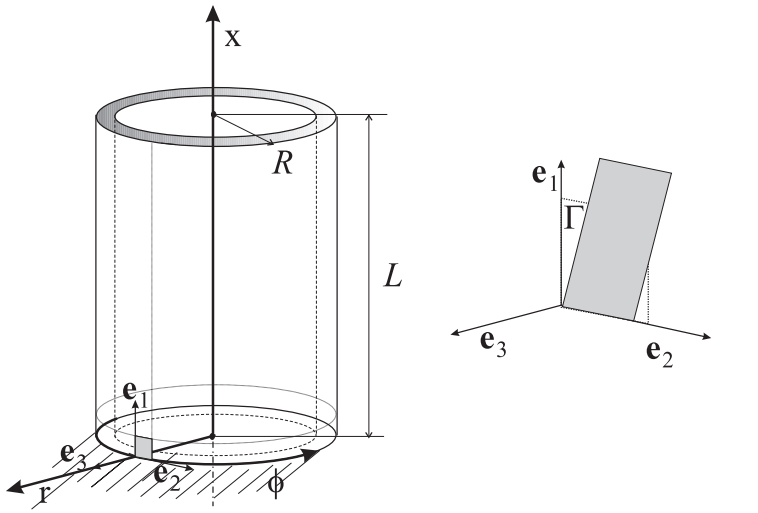

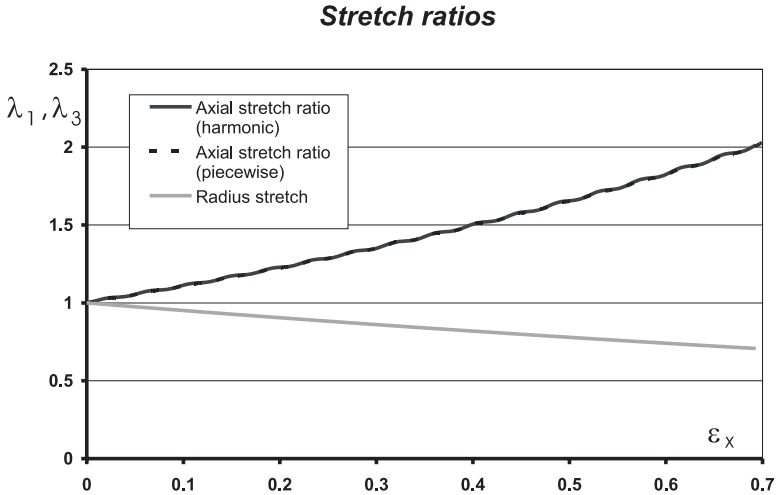

Fig. 1. Geometry of a cylindrical tube (up) and stretch ratios for tension assisted by cyclic torsion ($\eta = 6.56$, $E = 0.085$) (down)

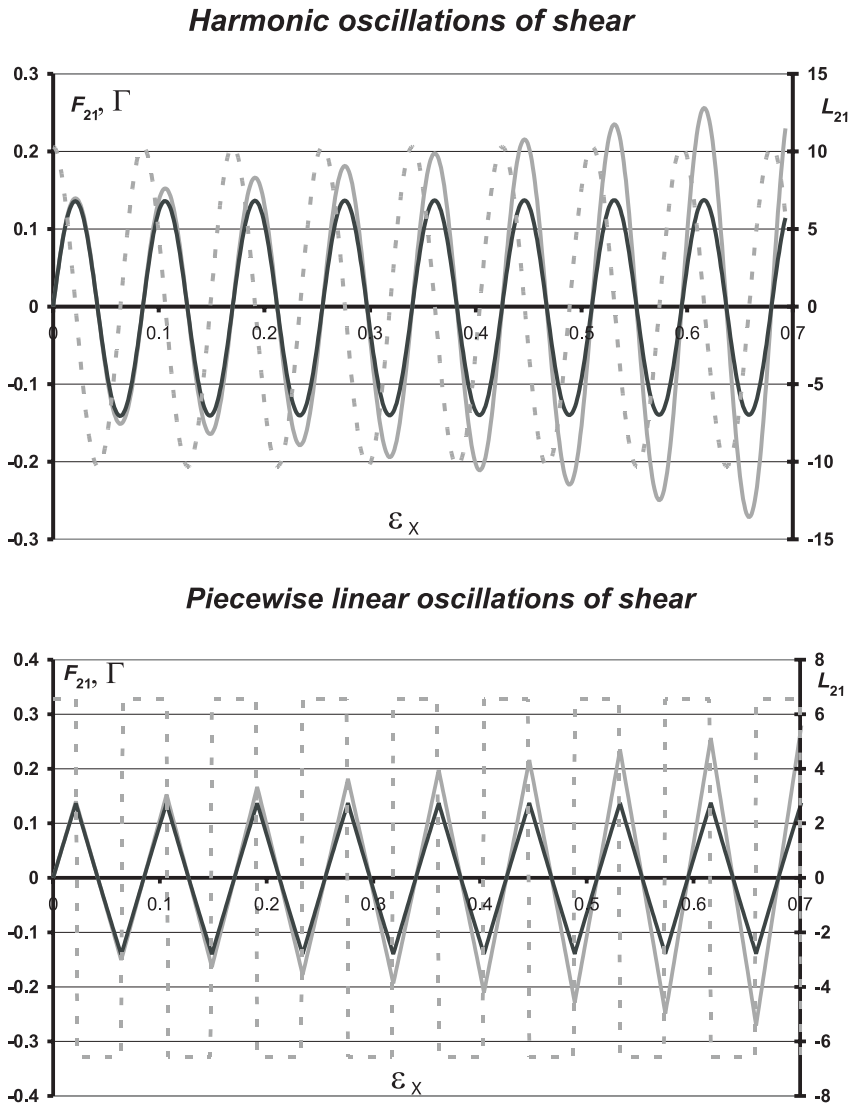

Fig. 2. Variation of component F_{21} of deformation gradient (solid grey line), L_{21} component od velocity gradient (dashed grey line) and shear angle Γ (solid black line) with ε_x ($\eta = 6.56$, $E = 0.085$)

3.2. Results

In this subsection first the results of simulations concerning stress-strain curves will be presented and next the crystallographic texture development will be discussed.

3.2.1. Strain-stress curves

In Fig. 3 the variation of axial component of the macroscopic Cauchy stress Σ_{11} with F_{11} component of deformation gradient are presented for the compression assisted by cyclic torsion. The material model discussed in subsection 2.1 has been applied. The following values of the material parameters have been identified in [14] with use of the experimental results for polycrystalline copper [1, 9]

$$n = 20, \quad \tau_{c0} = 14MPa, \quad h_0 = 232.75MPa,$$

$$\tau_{sat} = 138.6MPa, \quad q = 1.4, \quad \beta = 2.5.$$

Gradual reduction of the value of Σ_{11} is observed with the increasing value of the parameter η_o. Also, for larger shear strain amplitude γ_m the reduction of axial stress is more pronounced.

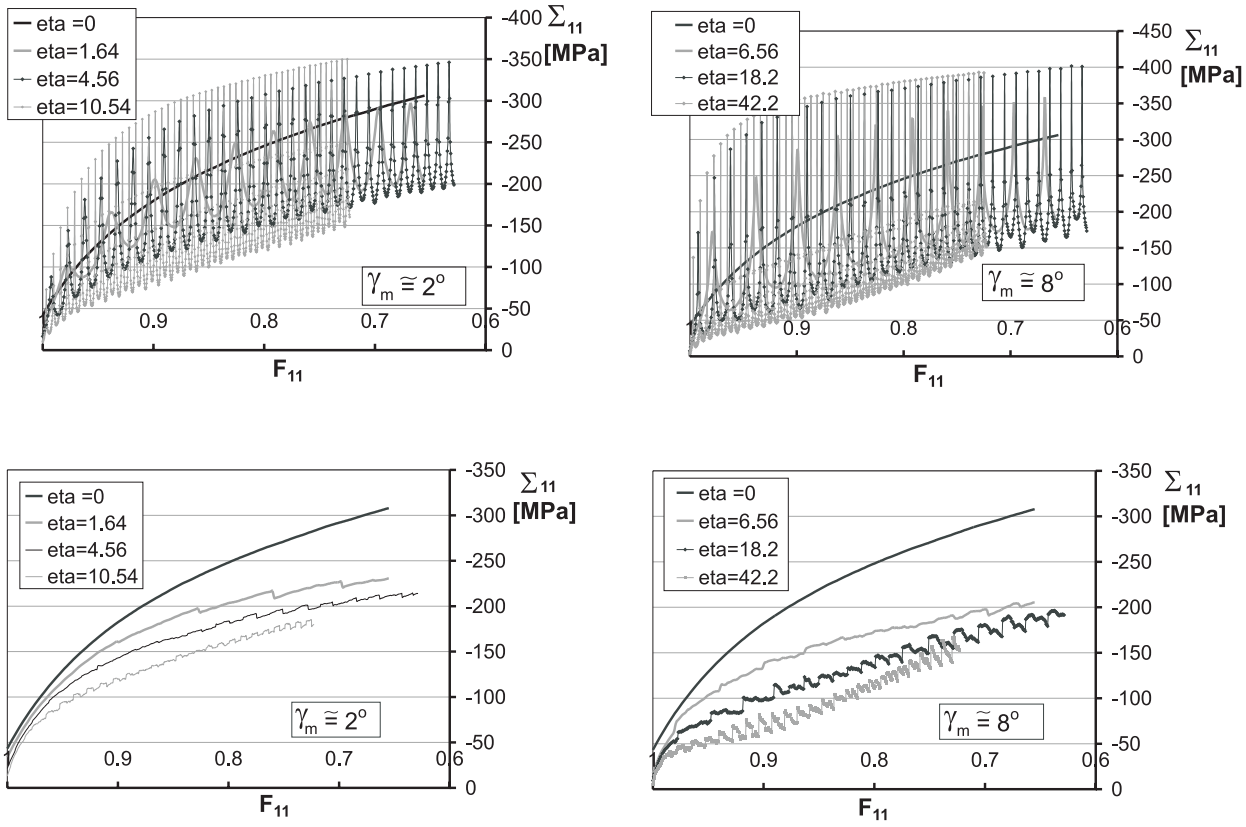

Fig. 3. Variation of axial component of the macroscopic Cauchy stress with F_{11} for compression assisted by harmonic torsion oscillations (upper row) and piecewise linear torsion oscillations (lower row), *eta* = η_o in the labels of curves

These results have been recalculated to obtain variation of compressive axial force F with cylindrical tube shortening u. The initial cross-section A_0 and initial length L_o of a tube was assumed as those used in Grosman experiments on cylinders [8]. The results are presented in Fig. 4. For $\eta_0 = 0$ quantitative agreement with those experiments were achieved while in other cases the results may be compared only qualitatively due to a different geometry of the analysed specimens (a cylindrical tube versus a cylinder)[1)]. The observed influence of controlling parameters on the axial force reduction in simulations corresponds to the one observed in experiments.

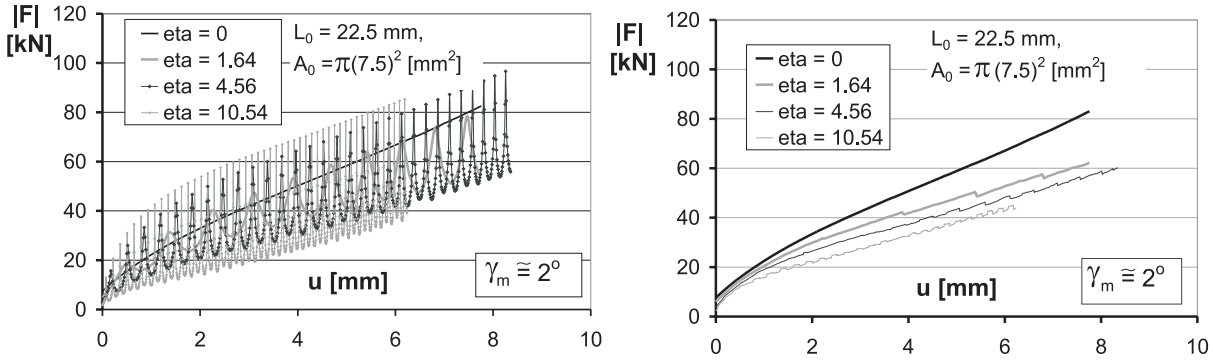

Fig. 4. Variation of compressive force with the cylindrical tube shortening for compression assisted by harmonic torsion oscillations (left) and piecewise linear torsion oscillations (right), *eta* = η_o in the labels of curves

[1)] Large number of considered grains makes the calculations time-consuming so that it is possible to perform analysis only at the material point or for a body that undergoes uniform deformation

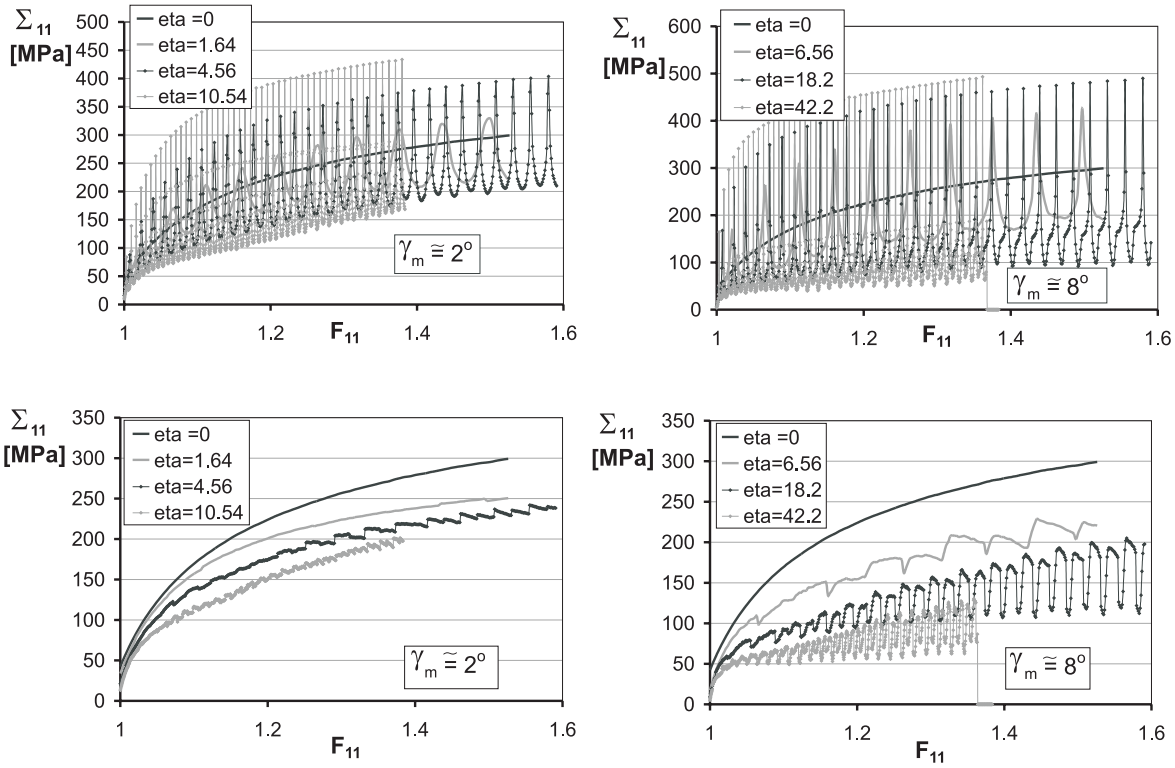

Fig. 5. Variation of axial component of the macroscopic Cauchy stress with F_{11} for tension assisted by harmonic torsion oscillations (upper row) and piecewise linear torsion oscillations (lower row), *eta* = η_o in the labels of curves

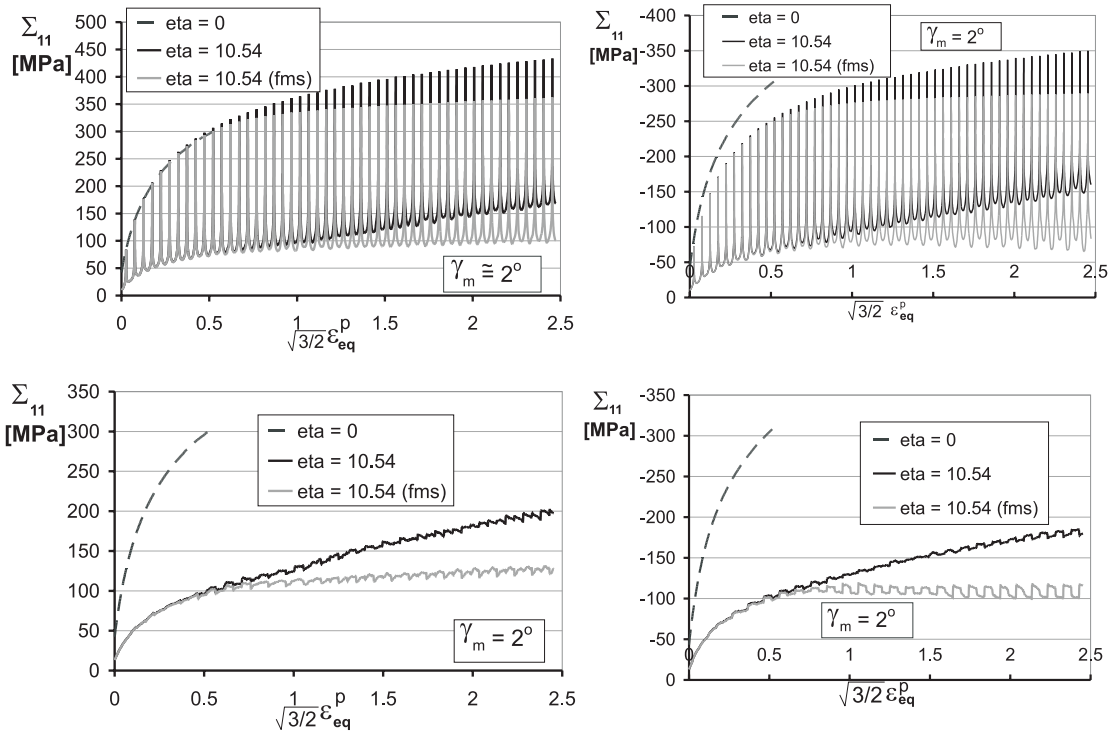

Fig. 6. Variation of axial component of the macroscopic Cauchy stress with the accumulated plastic strain ε_{eq}^{p} for tension (left) or compression (right) assisted by harmonic torsion oscillation (upper row) and piecewise linear torsion oscillation (lower row), *eta* = η_o in the labels of curves – the effect of incorporation of micro-shear banding

The same program of simulations has been also conducted for tension assisted by cyclic torsion. Due to the applied large strain formalism and the role of the plastic anisotropy induced by the texture development the results concerning the stress-strain curves for tension and compression differs contrary to what has been obtained in the case of small strain and the classical H u b e r-V o n M i s e s plasticity analysed in [15] for the same type of processes. In Fig. 5 the variation of macroscopic axial stress with F_{11} is presented. General tendency concerning the role of process parameters as well as the curve character is similar but some differences may be noticed in the shape of curves comparing to the compression process.

Now, let us look at the effect of incorporation of micro-shear banding mechanism of plastic deformation into the constitutive modelling on the axial stress reduction. The following material parameters for the function f_{MS} were identified with use of experimental data presented in [1, 9]

$$\alpha = 1.0, \quad f_{MS}^{\infty} = 0.85, \quad a = 5.0, \quad b = 9.62.$$

In Fig. 6 the variation of macroscopic axial stress with the equivalent plastic strain is presented. One may observe that in the process of tension or compression assisted by cyclic torsion the accumulated plastic strain is much larger than in the traditional process represented by the curve $\eta = 0$. Extension of the constitutive model accounting for the shear banding enables to obtain further reduction of axial stress comparing to the model without introduction of f_{MS} function.

We conclude this subsection with the presentation of the results concerning the plastic dissipation (Fig. 7). As it can be expected, similarly to the results in [15], with the increasing parameter η_o the plastic dissipation is also increasing. Some reduction of plastic dissipation due to the reduction of the strain hardening rate is obtained when applying the model with shear banding (Fig. 8).

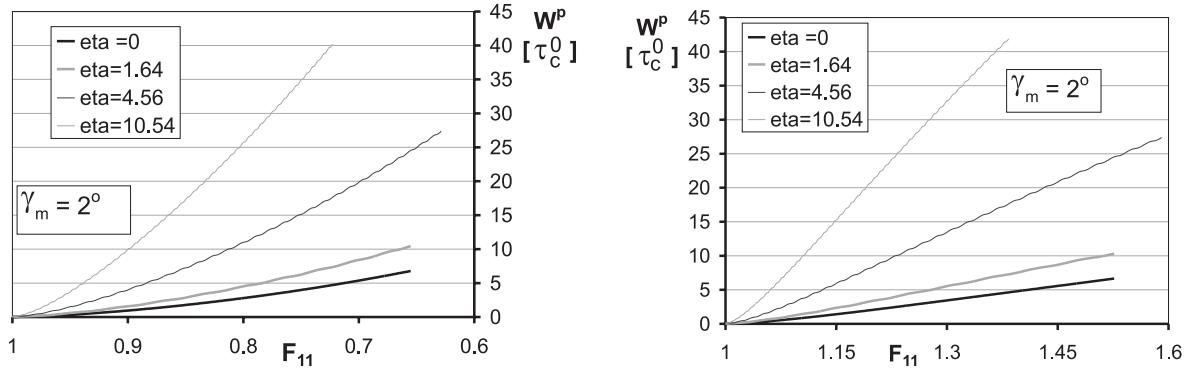

Fig. 7. Increase of plastic work during the process of compression (left) and tension (right) assisted by harmonic torsion oscillation, $eta = \eta_o$ in the labels of curves

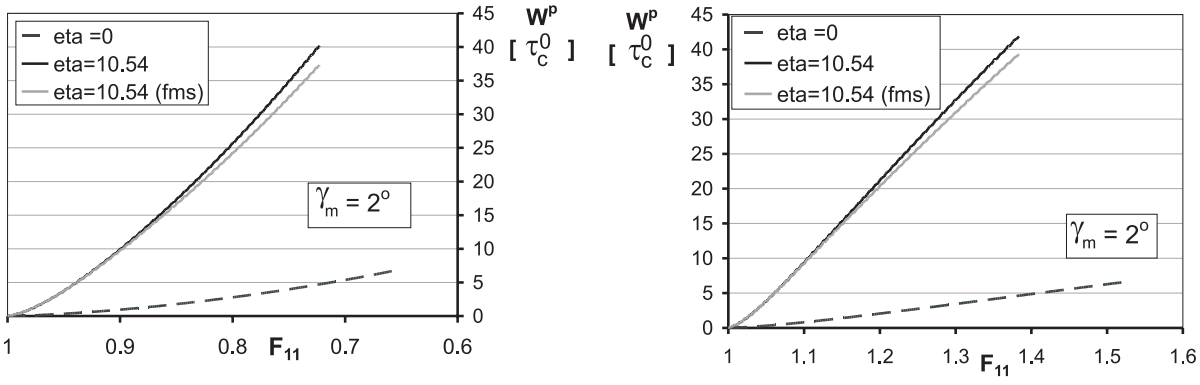

Fig. 8. Increase of plastic work during the process of compression (left) and tension (right) assisted by harmonic torsion oscillation – the effect of incorporation of shear banding, $eta = \eta_o$ in the labels of curves

3.2.2. Crystallographic texture development

In this subsection we will present the results concerning the crystallographic texture evolution in the analysed processes. In order to clarify the effects observed for the grain aggregate, first, we look at the behaviour of single, arbitrary selected orientation, Fig. 9.

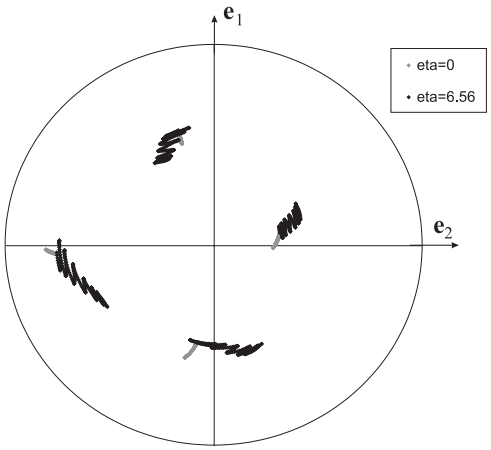

Fig. 9. Comparison of reorientation of arbitrary selected grain during the simple compression and compression assisted by cyclic torsion – standard pole figure {111}, *eta* = η_o in the labels of points

One may observe that the orientation path is different for the process assisted by cyclic torsion than for the simple compression. In the first case it is composed of reversible rotation connected with torsion and reorientation due to the compression. Furthermore, the final orientation of a grain differs from that achieved in the conventional process. It is due to the fact that in the analysed process the direction of strain rate tensor is completely different than in the simple compression/tension process so the plastic flow is executed by the different set of slip systems. Consequently, crystallographic texture developed in the analysed processes with non-proportional strain paths predicted by the crystal plasticity models differs significantly (Figs 10 and 11) from the widely reported textures of simple compression or extrusion (see for example [1]). Note that the applied model fairly well predicts these textures (compare Figs 10a and 11a).

When the effect of micro-shear banding is added, depending on the prescribed assumption (2.12), with increasing contribution of micro-shear banding the evolution of crystallographic texture is impeded or the final developed texture is changed with respect to the model without micro-shear banding, respectively. In Fig. 12 the second case is presented. The observation that in the presence of micro-shear bands the developed crystallographic texture is different [17, 22] may be explained by the localized character of plastic deformation. Outside the zones of micro-shear banding the rate of plastic deformation is much smaller than the averaged rate of plastic deformation in the whole volume element.

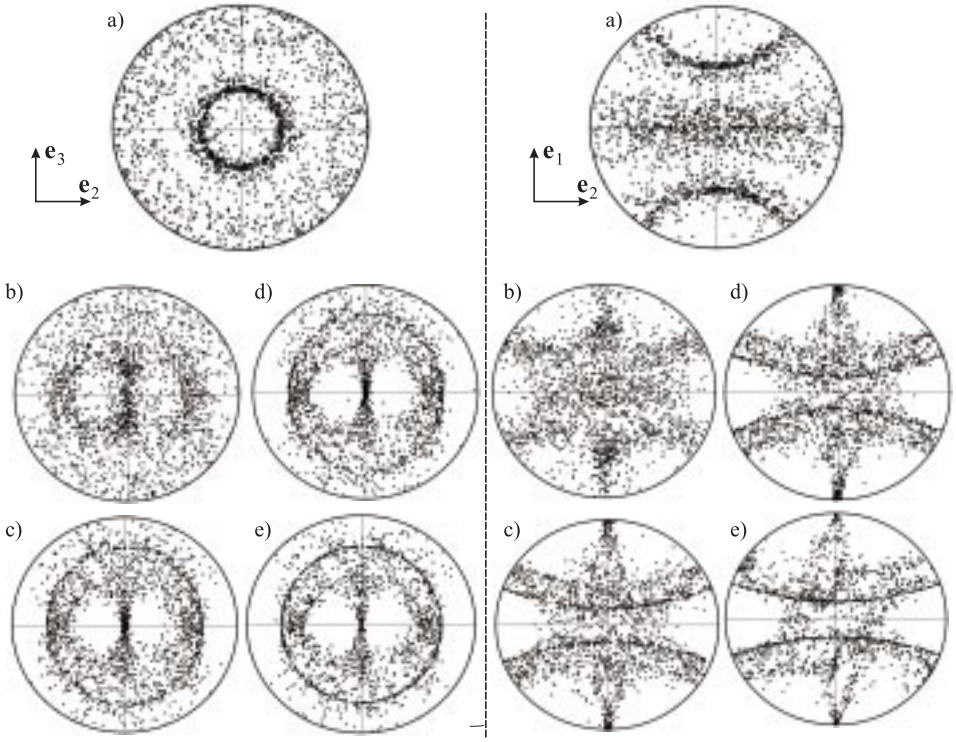

Fig. 10. Final standard pole figures {111} for compression assisted by harmonic torsion oscillations: a) $\eta_o = 0$, b) and c) $\gamma_m \simeq 2^o$, $\eta_o = 1.64$ and $\eta_o = 10.54$, d) and e) $\gamma_m \simeq 8^o$, $\eta_o = 6.56$ and $\eta_o = 42.2$

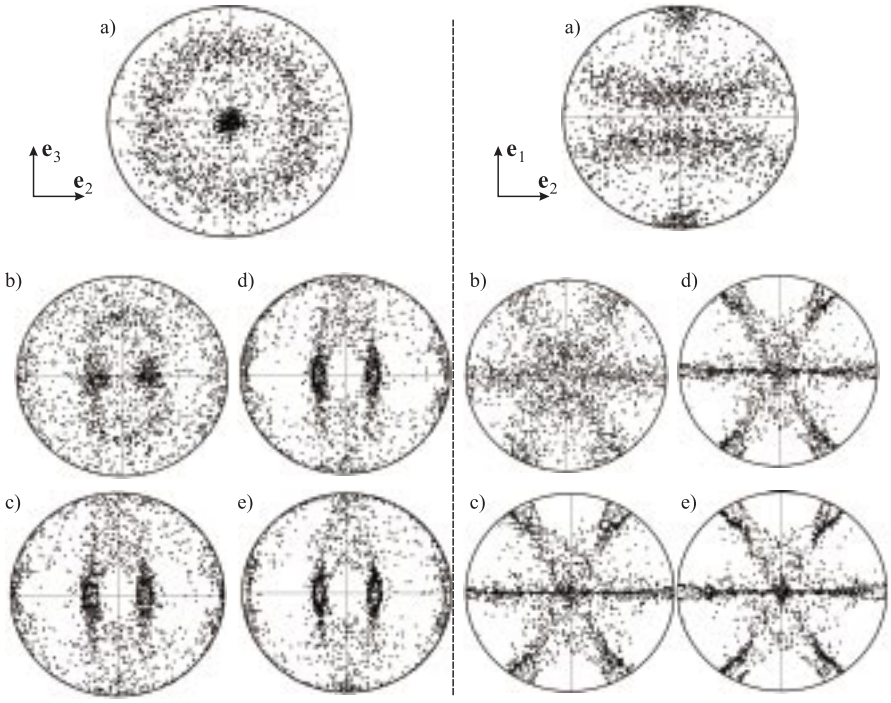

Fig. 11. Final standard pole figures {111} for tension assisted by harmonic torsion oscillations: a) $\eta_o = 0$, b) and c) $\gamma_m \simeq 2^o$, $\eta_o = 1.64$ and $\eta_o = 10.54$, d) and e) $\gamma_m \simeq 8^o$, $\eta_o = 6.56$ and $\eta_o = 18.2$

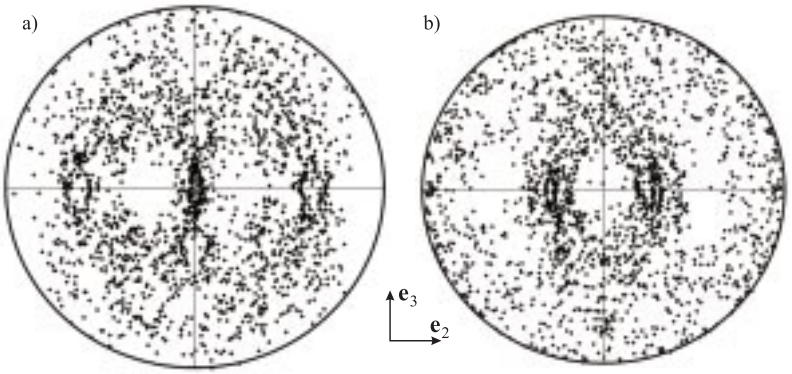

Fig. 12. Final standard pole figures {111} for tension (a) and compression (b) assisted by harmonic torsion oscillations, $\gamma_m \simeq 2^o$, $\eta_o = 10.54$ – effect of micro-shear banding ($\bar{f}_{MS} = f_{MS}$)

4. Conclusions

The polycrystalline behaviour and texture development have been studied for the advanced plastic deformation processes with non-proportional strain paths, namely tension or compression assisted by torsional oscillations. The crystal plasticity model with one yield surface expressed by the homogeneous yield function of degree $2n$ has been applied within large strain formalism. In order to account for the effect of micro-shear banding mechanism on the reduction of the strain rate hardening the simplified model developed in [13] has also been applied.

The applied micromechanical model enables also to simulate the crystallographic texture development that is a result of lattice rotation within the grain aggregate subjected to large plastic deformations. The theoretically obtained crystallographic texture evolution in the analysed processes is significantly different than that predicted for the simple compression or extension. The reason is the fact that in the crystal plasticity framework the texture evolution strongly depends on the set of deformation mechanisms constituting the deformation path (compare Eqs. (2.1), (2.5)). It must be stressed that the success in the texture prediction lies in the proper reproduction of the deformation path in the analysed process together with the knowledge of the potential set of deformation mechanisms for the considered material. The experimental measurements of texture development in the processes with non-proportional deformation paths should serve

as a tool for verification of this input information and the applied micromechanical model.

Two controlling parameters for the analysed deformation programs, γ_m and η_o, affect the process as follows: the higher γ_m and η_o the more significant is the axial stress reduction. In the same time the plastic work is always increased as compared to the processes without torsional oscillations. These conclusions correspond to the results of theoretical analysis performed in [15] in the case of phenomenological plasticity theory. It should be stressed that the results of simulations presented in this paper are not directly comparable to the situation met in the KOBO process of extrusion assisted by cyclic torsion. In the simulated process the whole sample undergoes plastic deformation while in the KOBO process the zone of plastic yielding is strongly localized.

Acknowledgements

Most of the results reported in the paper was obtained in the framework of the research project No. PBZ-KBN-102/T08/2003 supported by the State Committee for Scientific Research of Poland.

REFERENCES

[1] L. Anand, Single-crystal elasto-viscoplasticity, application to texture evolution in polycrystalline metals at large strain. *Comput. Methods Appl. Mech. Engrg.* **193**, 5359-5383 (2004).

[2] L. Anand, S. R. Kalidindi, The process of shear band formation in plane strain compression of fcc metals: Effects of crystallographic texture, MECH. MATER. **17**, 223-243 (1994).

[3] R. J. Asaro, Crystal plasticity. J. APPLIED MECHANICS **50**, 921-934 (1983).

[4] R. J. Asaro, A. Needleman, Textured development and strain hardening in rate dependent polycrystals, ACTA METALL. **33**(6), 923-953 (1985).

[5] W. Bochniak, K. Marszowski, A. Korbel, Theoretical and practical aspects of production of thin-walled tubes by the KOBO method, J. MATER. PROC. TECHNOL., **169**, 44-53 (2005).

[6] Y. F. Dafalias, Orientational evolution of plastic orthotropy in sheet metals, J. MECH. PHYS. SOLIDS, **48**, 2231-2255 (2000).

[7] W. Gambin, Refined analysis of elastic-plastic crystals, INT. J. SOLIDS STRUCTURES, **29**(16), 2013-2021 (1992).

[8] F. Grosman, J. Pawlicki, The impact of compression with oscilatory torsion parameters on technological plasticity of metals [in Polish], RUDY I METALE NIEŻELAZNE, **R50**(10-11), 590-594 (2005).

[9] S. R. Kalidindi, L. Anand, Macroscopic shape change and evolution of crystallographic texture in pre-textured fcc metals, J. MECH. PHYS. SOLIDS, **42**, 459-490 (1994).

[10] A. Korbel, W. Bochniak, The structure based design of metal forming operations, J. MATER. PROC. TECHNOL., **53**, 229 (1995).

[11] A. Korbel, W. Bochniak, Refinement and control of metals structure elements by plastic deformation, SCRIPTA METAR., **51**, 755-759 (2004).

[12] K. Kowalczyk, W. Gambin, Model of plastic anisotropy evolution with texture-dependent yield surface, INT. J. PLASTICITY, **20**, 19-54 (2004).

[13] K. Kowalczyk-Gajewska, W. Gambin, R. B. Pęcherski, J. Ostrowska-Maciejewska, Modelling of crystallographic texture development in metals accounting for micro-shear banding, ARCH. METALL. MATER., **50**, 575-593 (2005).

[14] K. Kowalczyk-Gajewska, R. B. Pęcherski, Micromechanical modeling of polycrystalline materials, CD ROM PROCEEDINGS OF PLASTICITY'06, 17-22 JULY 2006, Halifax, 2006.

[15] Z. Mróz, K. Kowalczyk-Gajewska, J. Maciejewski, R. B. Pęcherski, Tensile or compressive plastic deformation assisted by cyclic torsion, ARCH. MECH., **58** (2006).

[16] Z. Nowak, R. B. Pęcherski, Plastic strain in metals by shear banding. II. Numerical identification and verification of plastic flow accounting for shear banding, ARCH. MECH., **54**, 621-634 (2002).

[17] H. Paul, Z. Jasieński, A. Piątkowski, A. Litwora, A. Pawełek, Crystallographic nature of shear bands in polycrystalline copper, ARCH. METALL., **41**, 337-353 (1996).

[18] R. B. Pęcherski, Modelling of large plastic deformation based on the mechanism of micro-shear banding. Physical foundations and theoretical description in plane strain, ARCH. MECH., **44**, 563-584 (1992).

[19] R. B. Pęcherski, Continuum mechanics description of plastic flow produced by micro-shear banding, TECHNISCHE MECHANIK, **18**, 563-584 (1998).

[20] R. B. Pęcherski, Macroscopic effects of microshear banding in plasticity of metals, ACTA MECHANICA, **131**, 203-224 (1998).

[21] R. B. Pęcherski, K. Korbel, Plastic strain in metals by shear banding. I. Constitutive description for simulation of metal shaping operations, ARCH. MECH., **54**, 603-620 (2002).

[22] F. Stalony-Dobrzański, W. Bochniak, Role of shear bands in forming the texture image of deformed copper alloy, ARCH. METALL. MATER., **50**, 1089-1102 (2005).

Received: 10 March 2007.